METEOROID AND DEBRIS PROPERTIES FROM THIN AND THICK TARGETS

D. J. Gardner and J. A. M. McDonnell

Unit for Space Sciences and Astrophysics, University of Kent at Canterbury,
Canterbury, Kent, CT2 7NR. UK.

ABSTRACT

Impacts on the thin foils of the Micro-Abrasion Package (MAP) on NASA's LDEF satellite and the Timeband Capture Cell Experiment (TiCCE) on ESA's Eureca satellite produce holes which are primarily related to the profiles ("diameters") of impacting micro-meteoroids and space debris particles. Combining these data with impact data from thick target impact craters, for which the damage more dependent on additional factors, and where such targets have experienced a statistically identical flux, leads to a measure of the impactor density which is only weakly affected by the assumed impact velocity. The actual mean density of the particles may then be found by using impact equations and statistical techniques to determine the effect of a density distribution.

This technique leads to a mean in the range 2.0–2.4 g/cm^{-3} in the ballistic limit range 5–1000 μm which corresponds to a mass range of approximately 10^{-9}–10^{-14} kg.

Comparison of the flux levels on the two spacecraft shows that in this size range the particles are primarily of interplanetary origin, although at the smaller end of the range orbital particles dominate.

1. NOTATION AND MEASUREMENTS

d_p	particle diameter	f	foil thickness
D_h	hole diameter	T_c	crater depth
D_c	crater diameter	F_{max}	ballistic limit
V	velocity	θ	impact Angle
ρ	density	σ	yield strength
S	standard deviation		

All measurements are relative to, or in, the original surface plane, except for D_h which is measured at the smallest diameter and θ which is relative to the surface normal. The ballistic limit, F_{max}, is defined as the maximum thickness of foil that the particle would perforate. Measurements are shown in Fig. 1.

2. INTRODUCTION

The determination of particle densities from hypervelocity impact craters has been performed for several decades (Ref. 1, 2, 3, for example) however these approaches have typically relied upon an assumed impact velocity to determine the density. Using a

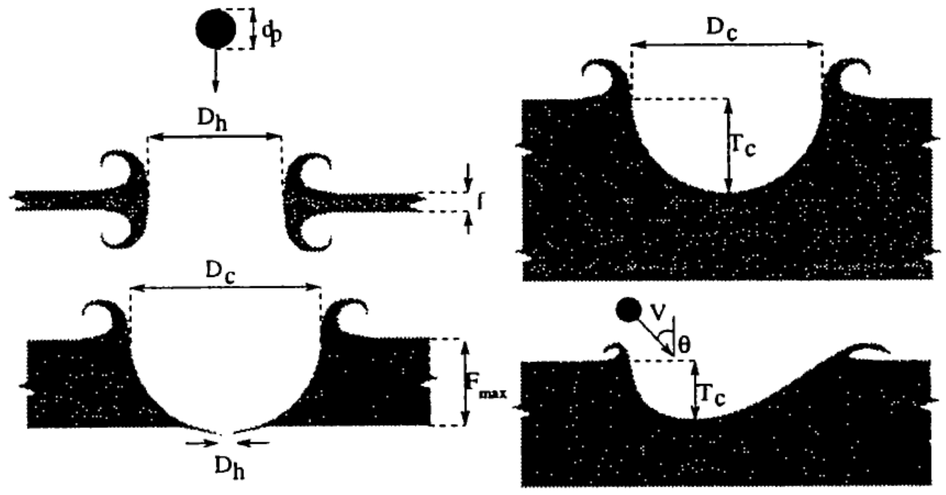

Figure 1: Measurements taken from a hypervelocity impact.

combination of impacts from thin and thick targets, however, combines a pair of impact relationships, and thus we find that some of the parameters are cancelled out to a large degree.

This approach has been taken previously by Paley (Ref. 4) and Deshpande (Ref. 5), unfortunately these works made use of the equation of Carey et al. (Ref. 6), which does not represent the marginal perforation regime well. They also failed to consider the effects of a distribution of impactor densities and velocities.

3. THE GMC EQUATION

The hole growth equation of Gardner, McDonnell and Collier (Ref. 7) (or GMC equation) is unusual in that rather than giving the hole diameter caused in a given foil by a known particle, it gives the diameter of the particle that caused a known hole. This approach better represents the situation with the analysis of space-flown foils and also greatly simplifies the mathematics. In the context of this work it also permits the determination of F_{max} as a function of D_h for an impacting particle.

The equation takes the form:

$$\frac{d_p}{f} = A\left(\frac{10}{9+e^{\frac{D_h}{fB}}}\right) + \frac{D_h}{f}\left(1-e^{-\frac{D_h}{fB}}\right) \qquad (1)$$

where A and B are dependent on the projectile and target materials and parameters. The values of A and B (for an aluminium target) are given in Eqs. 2 & 3. Where f is in μm and all other units are in SI.

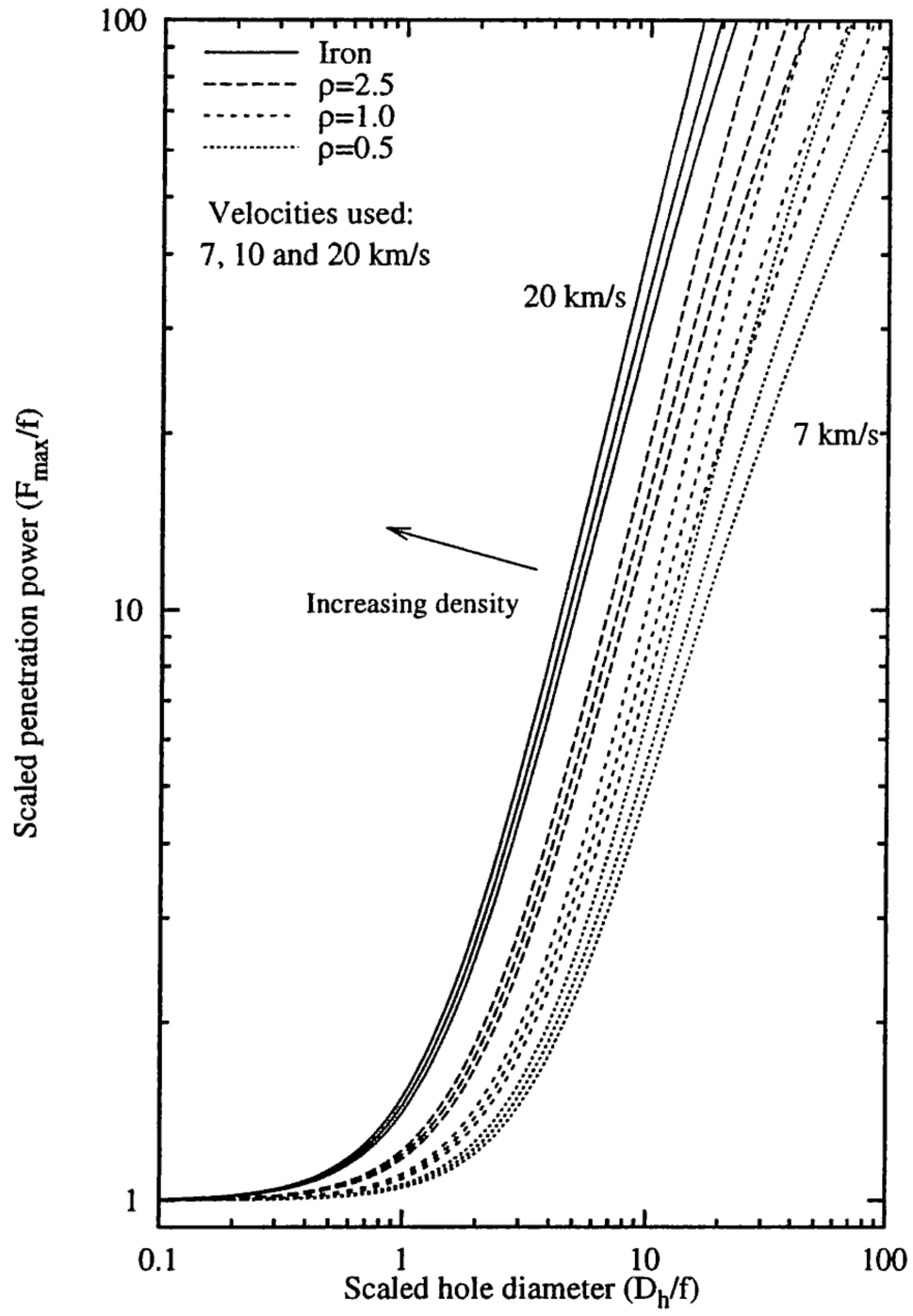

Figure 2: The modified GMC equation for a variety of impactor velocities and densities.

$$A = 6.97 \left(\frac{V \rho_p}{\sqrt{\sigma_t \rho_t}} \right)^{-0.723} \left(\frac{\sigma_t}{\sigma_{Al}} \right)^{-0.217} f^{-0.053} \quad (2)$$

$$B = \begin{cases} V \leq 6.0\,\mathrm{km/s} : 1.85 \times 10^{-3} V - 0.004 \\ V > 6.0\,\mathrm{km/s} : 0.74 \times 10^{-3} V + 6.66 \end{cases} \quad (3)$$

4. APPLICATION TO IMPACT DATA

Since A represents the limiting case of zero diameter hole, and is thus in fact d_p/F_{max}, we can divide by this to get the relationship of Eq. 4, shown in Fig. 2.

$$\frac{F_{max}}{f} = \left(\frac{10}{9 + e^{\frac{D_h}{fB}}} \right) + \frac{D_h}{fA} \left(1 - e^{-\frac{D_h}{fB}} \right) \quad (4)$$

Fig. 2 shows that whilst impact velocity has an effect on the relationship, it is not as significant as density. Comparing these graphs with an "actual" D_h to F_{max} relationship (Fig. 3) obtained from the

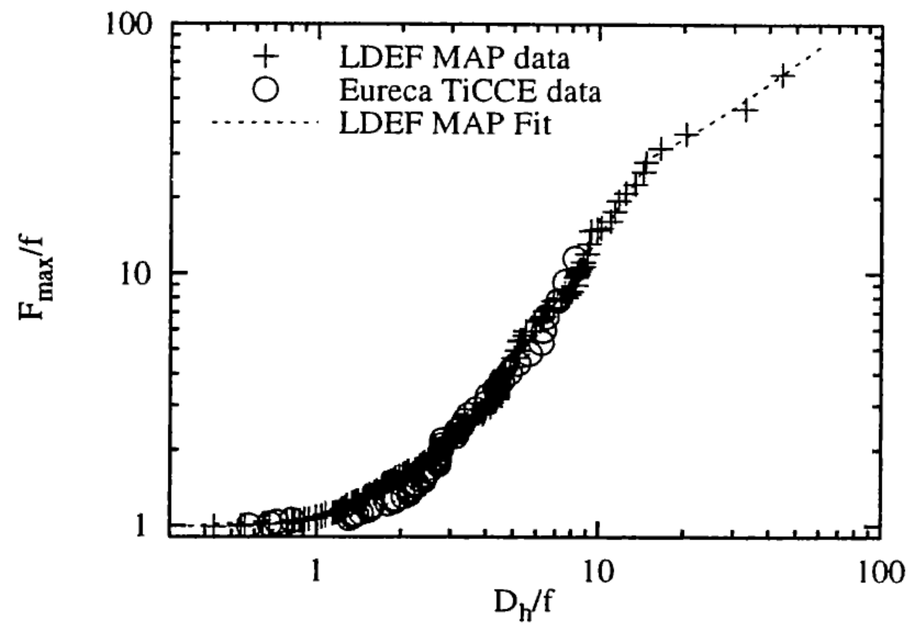

Figure 3: Spacecraft D_h to F_{max} relationships obtained by Gardner et al. (Ref. 8).

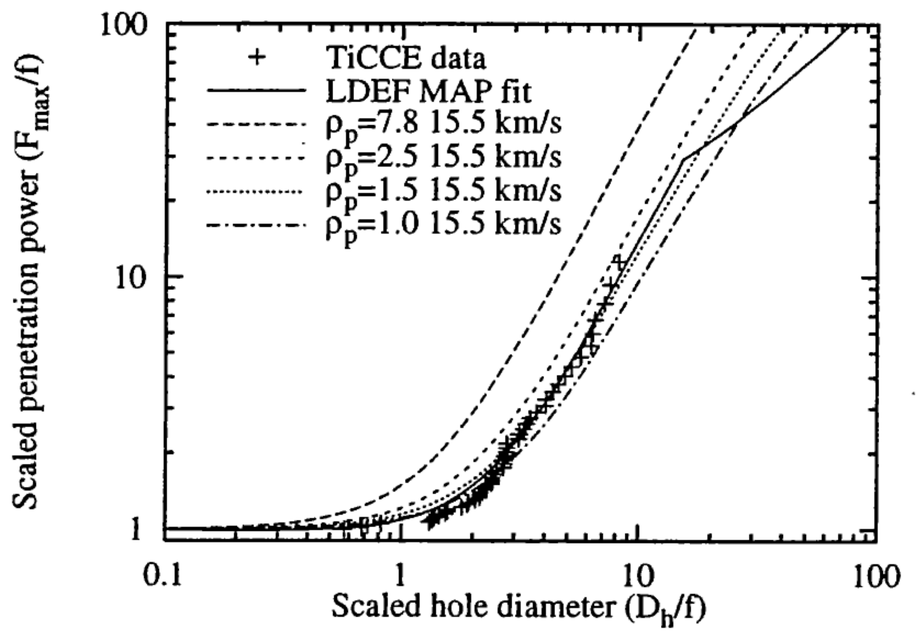

Figure 4: Comparison of spacecraft D_h to F_{max} relationships with curves from Eq. 4.

Space face MAP and TiCCE experiments (Ref. 8) we find (Fig. 4) that the in-situ data corresponds to impacts from particles of density 1.5 g/cm^3.

The effect of a distribution of densities (and velocities), however, must not be ignored, as in general $\overline{f(x)} \neq f(\bar{x})$. A computational approach has therefore been used to simulate these effects. Distributions published by Babadzhanov (Ref. 9) for (sporadic and stream) photographic meteors and by Love et al. (Ref. 10) and Flynn and Sutton (Ref. 11)[1] from stratospheric particles were used with densities for a particular simulation run chosen randomly from the selected distribution. Velocities were similarly selected from the distribution of Taylor (Ref. 12), and particle sizes were selected so as to generate a "realistic" flux distribution.

The results of a typical set of simulations is shown in Fig. 5. The mean densities of the impactors in this

[1]Flynn and Sutton deliberately selected "fluffy agglomerates" for their study.

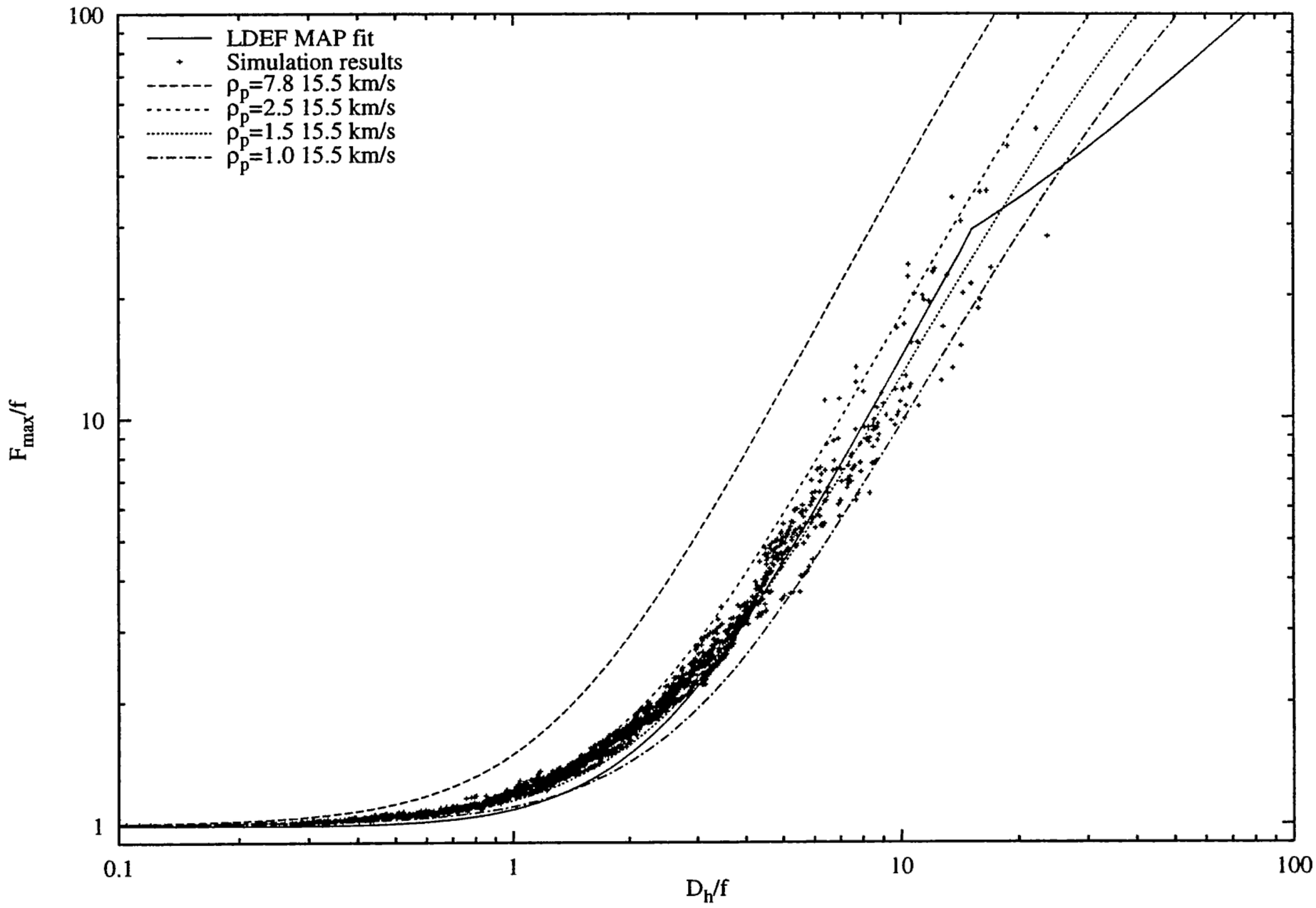

Figure 5: Simulation results using Taylor's velocity distribution and Babadzhanov's density distribution.

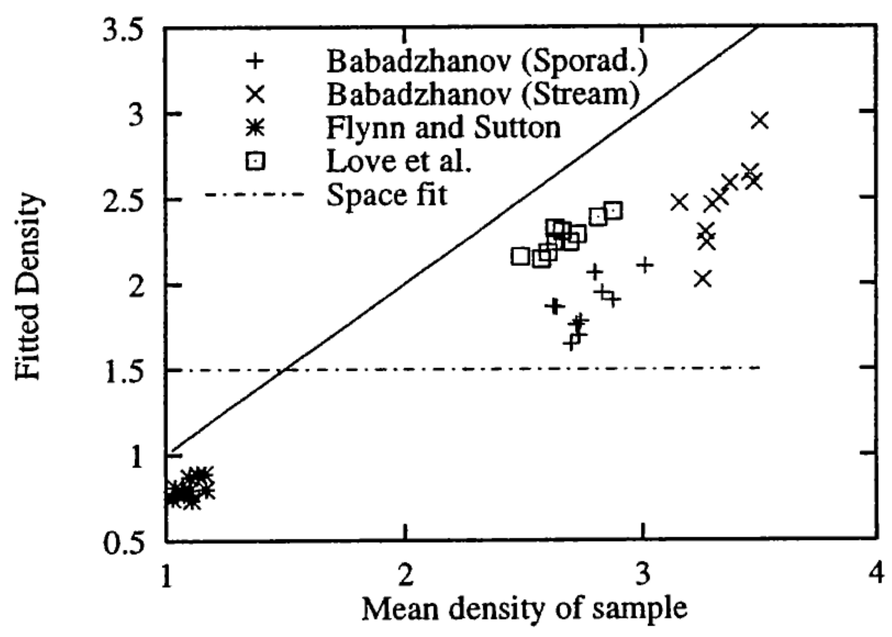

Figure 6: Simulation results compared to the true sample mean for a variety of distributions.

set of simulations were in the range $2.4 < \bar{\rho} < 2.9$, whereas the density obtained from fitting equation 4 was found to be in the range $1.4 < \rho < 1.7$. Similar calculations were performed and the relationship between the sample mean and the fit is shown in Fig. 6

This marked divergence between the fit and the true mean led to further studies, in which the mixing ratio of a bimodal distribution, and the width of a monomodal density spectrum were altered. Figure 7 shows that the method used is sensitive to low density particles, and that only a small fraction of low density particles can have a significant effect on the fitted density. Figure 8 shows that with increasing standard deviation (S) of the input density distribution there is a marked decrease in the fitted density, and also that this effect is not significantly affected by the shape or the mean density (ρ) of the distribution. We thus find that the ratio (S/ρ) of the standard deviation to the mean of the impacting particle densities gives a reasonable measure of the "de-rating ratio" (R) i.e. the ratio of the fitted density to the mean density. The fitted line is given in Eq. 5.

$$R = 1 + 5.33 \times 10^{-2} \left(1 - \exp\left(3.15\frac{S}{\rho}\right)\right) \qquad (5)$$

Table 1 shows the normalised standard deviation (S/ρ) for the published distributions considered here, and the de-rating ratio expected (from Eq. 5) for these distributions. For an apparent mean of 1.5 g/cm^3, and assuming that Eq. 5 holds and the published density distributions considered are of representative width, the true mean density is in the range 2.0–2.4 g/cm^3.

Distribution	$\bar{\rho}$ (g cm^{-3})	S (g cm^{-3})	S/ρ	De-rating ratio (R)
Babadzhanov (sporadics)	2.7	1.8	0.66	0.63
Babadzhanov (stream)	3.3	1.8	0.56	0.74
Love et al.	2.4	1.1	0.56	0.74
Flynn & Sutton	1.1	0.63	0.57	0.73

Table 1: De-rating factor expected from published density distributions.

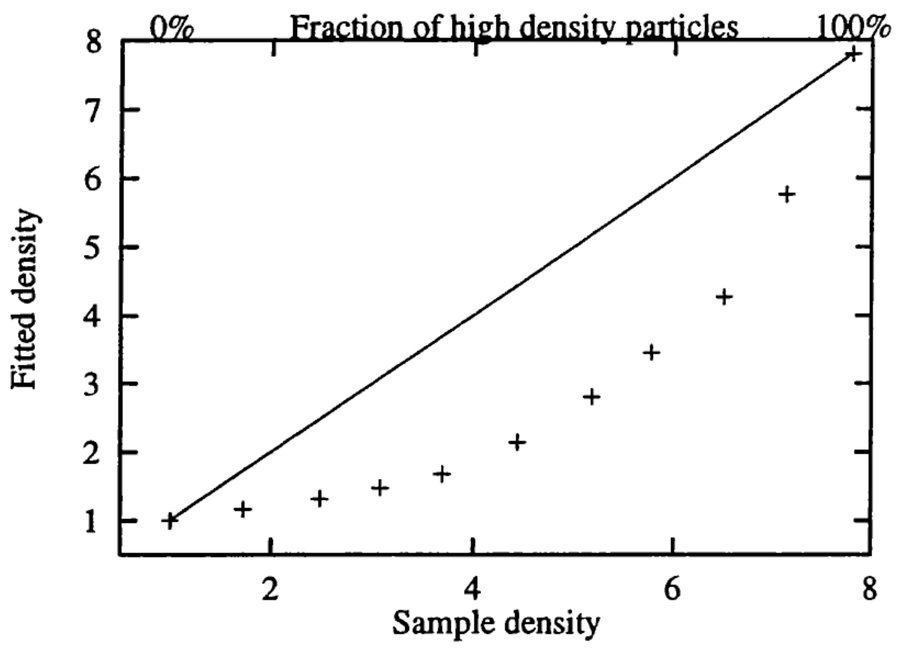

Figure 7: Fitted density obtained from a bimodal distribution, as a function of the mixing ratio.

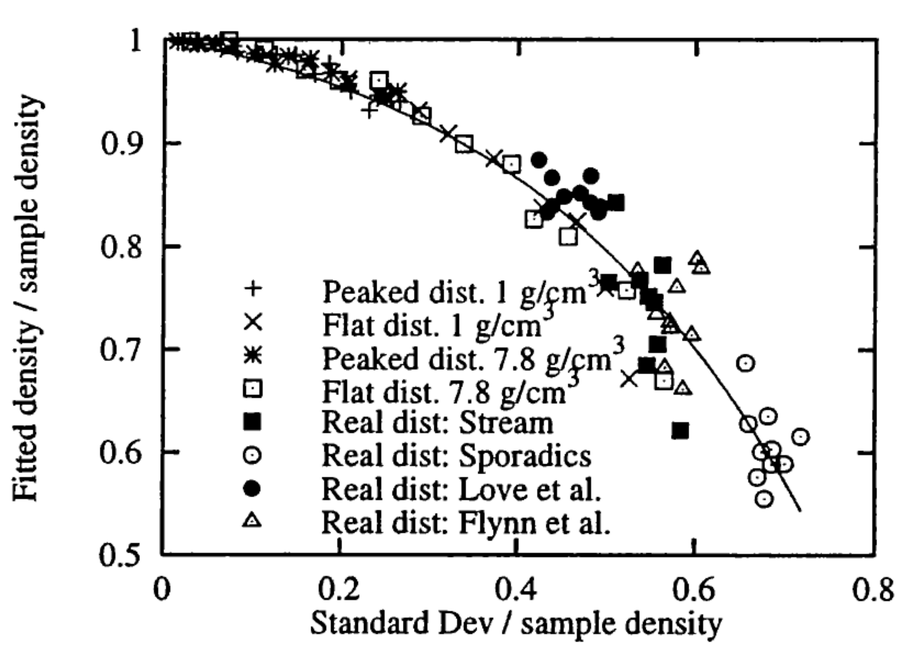

Figure 8: Effect of normalised standard deviation (S/ρ) on the de-rating ratio (fitted density / true density). Four idealised distributions are shown, as are those from (Ref. 9, 10, 11)

5. SOURCES OF IMPACTORS

It is normal to divide the possible impacts on a satellite in LEO into two main sources: natural and debris. Analyses of LDEF's impact flux record have concentrated on discriminating between this pair of sources, initially based upon the assumption that natural sources are either isotropic or are "smeared out" over the orbital lifetime of the satellite (Ref. 13), to become effectivly isotropic as far as the impact record is concerned. More recent work (Ref. 14) has shown that this assumption is not fully justified, at least as far as the North and South pointing faces are concerned.

The pointing attitude of EuReCa (stabilised with respect to the sun as opposed to spacecraft ram direction for LDEF) produces a random exposure to debris, however any enhancement of the natural particle influx from the Earth-ram direction will be visible as an enhancement over the LDEF average. Thus in comparing LDEF's impact record with that of the EuReCa TiCCE experiment (Ref. 8) an alternative division is suggested: isotropic and anisotropic relative to the Earth-ram direction. Into the isotropic category will fall orbital particles (debris and aerocaptured natural particles) and any isotropic component of the natural population.

The impact flux on the TiCCE experiment compared to the LDEF average (Fig. 9) clearly shows that such a bias is indeed found. Analysis of these flux differences (Ref. 15, 16) shows the Earth-ram flux to dominate above $F_{max} = 30\,mu$m (up to the largest impact data available, about 1000 μm). Below this size there is a transition region, until at 10 μm the flux is dominated by anisotropic sources (with respect to the Earth's apex of motion).

Comparing the flux observed on TiCCE with that on the LDEF East face, shows that while at small sizes LDEF East has a higher impact flux, for large scale impacts an approximately equal flux is suggested. The influx from the Earth-ram direction at these penetration scales thus presents a danger to spacecraft operations of similar magnitude to that of the spacecraft-ram direction.

6. LDEF'S EAST FACE

LDEF East face (pointing in the spacecraft ram direction) must have, by dynamical considerations, received an impact flux from debris particles. Comparisons of impact data from this face with modelled meteoroid fluxes reliably show an excess of particles which can be best attributed to debris. Recent modelling work (Ref. 15, 16) has shown a good agreement with a natural particle dominated flux distribution

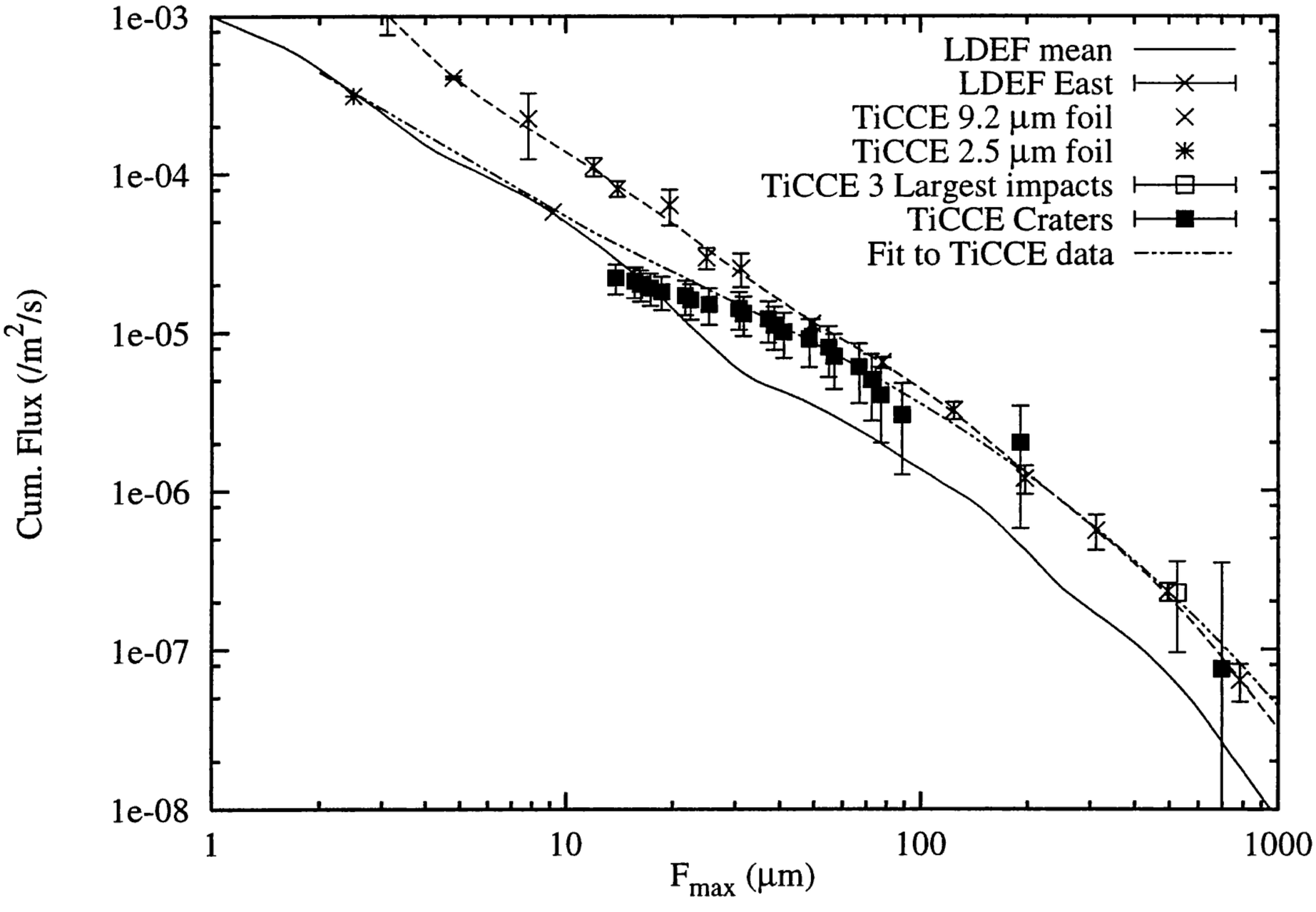

Figure 9: Impact flux on the EuReCa TiCCE experiment compared to that on LDEF.

at large sizes ($F_{max} > 50\,\mu$m), with an excess of particles at smaller sizes. This data shows agreement with the TiCCE data, and strongly suggests that below some 30–50 μm F_{max} most particles that impact on a satellite are orbital, and thus either debris or aerocaptured meteoroids (Ref. 17).

The result of treating data from the East face in a similar manner as that in Fig. 3 is shown in Fig. 10 for a variety of foil thicknesses. Fig. 11 compares these foil data to the curves and TiCCE data from Fig. 4. It is notable that, at small sizes, the data from both satellites drop below the curves (a feature not found in the Space face data considered earlier). The exact reason for this reduction is as yet unclear, but it has been found that similar effects may be obtained in the simulations by changing the velocity and density populations as a function of size, a situation we would expect for a change from a population dominated by natural particles to one dominated by orbital debris particles.

7. CONCLUSIONS

Meteoroid particles from the Earth's apex of motion are found to dominate the spacecraft flux for impacts capable of penetrating a foil of ~50 μm and above.

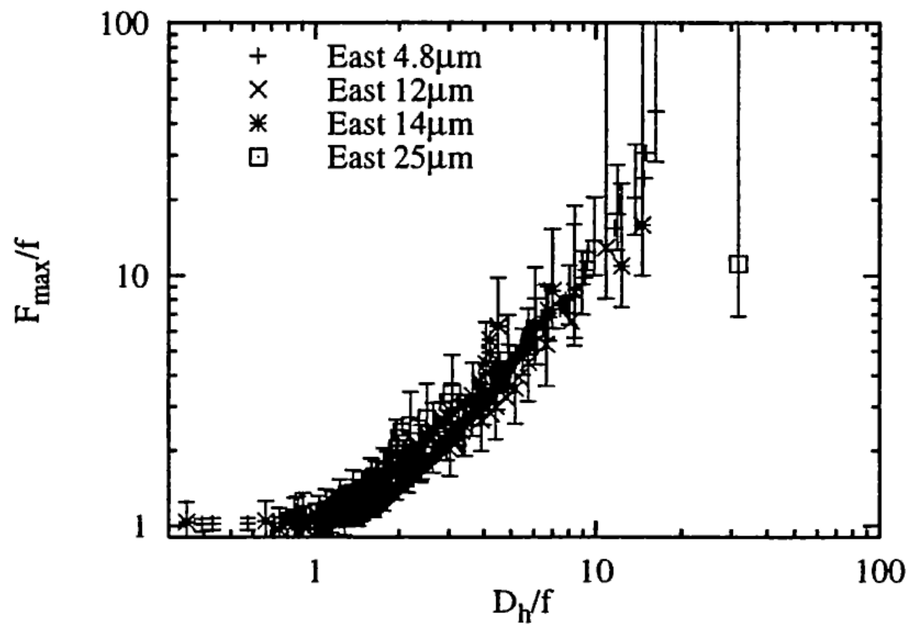

Figure 10: D_h to F_{max} relationships obtained from LDEF East face.

These particles are found to have a mean density in the range 2.0–2.4 g/cm^3.

The Earth-ram direction flux enhancement has been shown to give a flux of similar magnitude to that found for the spacecraft ram direction in these size ranges. It is thus appropriate, when spacecraft design is considered, to treat this flux source as seriously as that on the leading face.

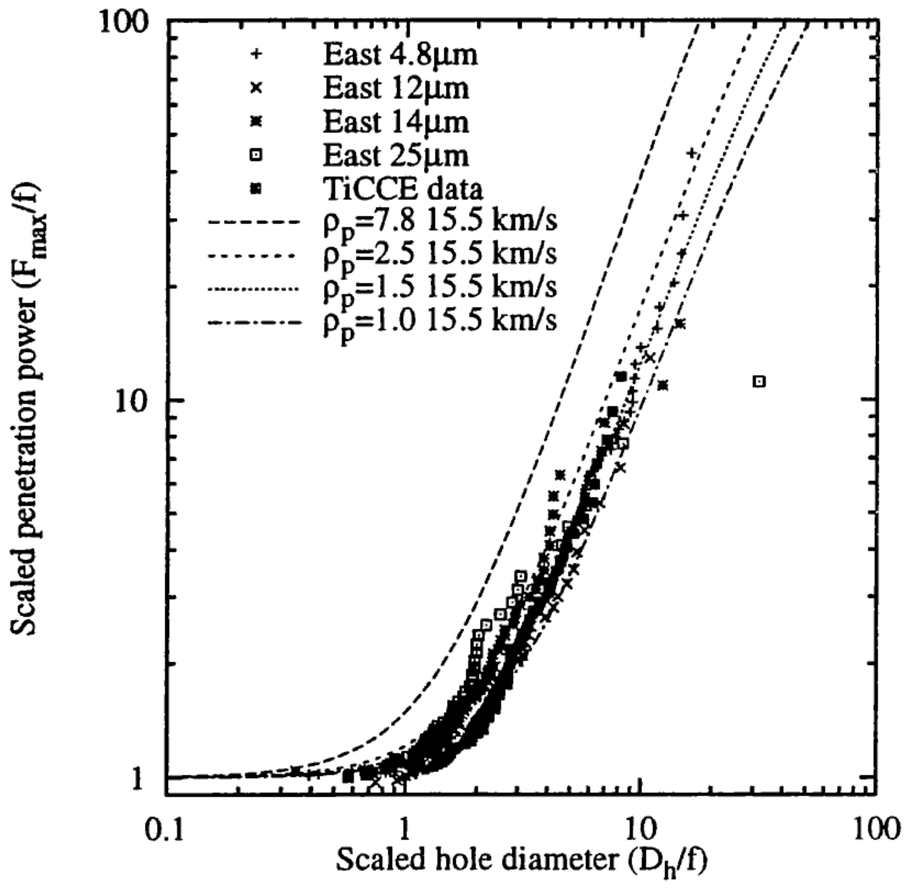

Figure 11: D_h to F_{max} relationships obtained from LDEF East face compared to the curves of Fig.4.

Analysis of surfaces exposed on spacecraft faces expected to receive a flux of debris particles, shows a feature consistent with a change in population density and/or velocity. Further analysis of this feature is the subject of an on-going study.

REFERENCES

1. Brownlee, D. et al., Some physical parameters of micrometeors, *Proc. 4th Lunar Sci. Conf.*, 3197–3312, 1974.

2. Brownlee, D. et al., Density, chemistry, and size distribution of interplanetary dust, *Proc. 6th Lunar Sci. Conf.*, 3409–3419, 1975.

3. Love, S. G. et al., Morphology of meteoroid and debris impact craters formed in soft metal targets on the LDEF satellite, *Int. J. Impact Engng.*, Vol. 16, No. 3, 405–418, 1995.

4. Paley, M. T., A refinement of hypervelocity impact equations using LDEF data, *Proc. 43rd Congress International Astronautical Federation*, 1992.

5. Deshpande, S. P., Ph.D. thesis, University of Kent at Canterbury, 1993.

6. Carey, W. C. et al., Capture cells: Decoding the impacting particle parameters, *Proc. XVIth Lunar and Planetary Science Conference (Abstracts volume)*, 111–112, LPSI Houston, 1985.

7. Gardner, D. J. et al., Hole growth characterisation for hypervelocity impacts in thin targets, *Int. J. Impact Engng.*, In press.

8. Gardner, D. J. et al., Micro-particle impact flux on the Timeband Capture Cell Experiment of the Eureca Spacecraft, *Adv. Space Res.*, Vol. 17, No. 12, 193–199, 1996.

9. Babadzhanov, P. B., Density of meteoroids and their mass influx on the earth., *Asteroids Comets, Meteors, Proc. IAU Symposium 160*, 45–54, 1994.

10. Love, S. et al., Densities of 5-15μm interplanetary dust particles., *Proc. 24th Lunar and Planetary Science Conference.*, 901–902, 1993.

11. Flynn, G. J. and Sutton, S. R., Evidence for a bimodal distribution of cosmic dust densities., *Proc. 21st Lunar Planet. Sci. Conf. (Abstracts volume).*, 375–376, 1991.

12. Taylor, A. D., The Harvard Radio Meteor Project meteor velocity distribution reappraised, *Icarus*, Vol. 116, 154–158, 1996.

13. Zook, H. A., Deriving the velocity distribution of meteoriods from the measured meteoroid impact directionality on the various LDEF surfaces, **LDEF — 69 Months in Space** *Proc. First Post-Retrieval Symposium*, editor A. S. Levine, Vol. 1, 569–579, NASA Conference Publication 3134, Kissimmee, Florida, 1991.

14. McBride, N. et al., Asymmetries in the natural meteoroid population as sampled by LDEF, *Planet. Space Sci.*, Vol. 43, No. 6, 757–764, 1995.

15. McDonnell, J. A. M. and Gardner, D. J., Recent near Earth satellite flux data: contributions in the definition of the interplanetary flux at 1 A.U. heliocentric distance., *Physics, Chemistry and Dynamics of Interplanetary Dust.*, editors B. A. S. Gustafson and M. S. Hanner, 1996, ASP Conference Series Vol. 104.

16. McDonnell, J. A. M. et al., Chapter 4: Near earth environment, *Interplanetary Dust*, editors S. Dermott, E. Grün, H. Fechtig and G. Gustafon, University of Arizona Press, submitted 1996.

17. Ratcliff, P. R. et al., The relative efficiency of aerocapture for interplanetary dust by the planets, *Planet. Space Sci.*, Vol. 41, No. 8, 603–608, 1993.